Temperature as a potent driver of regional forest drought stress and tree mortality

A. Park Williams[1]*, Craig D. Allen[2], Alison K. Macalady[3,4], Daniel Griffin[3,4], Connie A. Woodhouse[3,4], David M. Meko[4], Thomas W. Swetnam[4], Sara A. Rauscher[5], Richard Seager[6], Henri D. Grissino-Mayer[7], Jeffrey S. Dean[4], Edward R. Cook[6], Chandana Gangodagamage[1], Michael Cai[8] and Nate G. McDowell[1]

As the climate changes, drought may reduce tree productivity and survival across many forest ecosystems; however, the relative influence of specific climate parameters on forest decline is poorly understood. We derive a forest drought-stress index (FDSI) for the southwestern United States using a comprehensive tree-ring data set representing AD 1000–2007. The FDSI is approximately equally influenced by the warm-season vapour-pressure deficit (largely controlled by temperature) and cold-season precipitation, together explaining 82% of the FDSI variability. Correspondence between the FDSI and measures of forest productivity, mortality, bark-beetle outbreak and wildfire validate the FDSI as a holistic forest-vigour indicator. If the vapour-pressure deficit continues increasing as projected by climate models, the mean forest drought-stress by the 2050s will exceed that of the most severe droughts in the past 1,000 years. Collectively, the results foreshadow twenty-first-century changes in forest structures and compositions, with transition of forests in the southwestern United States, and perhaps water-limited forests globally, towards distributions unfamiliar to modern civilization.

Recent declines in forest productivity and tree survival have been documented at many sites globally and attributed to water limitation[1,2]. Forest declines may be accelerating in many regions because warming has amplified water limitation[3–10]. We describe forest declines due to water limitation as drought-induced declines, whether by lack of precipitation or by increased evaporative demand. In the southwestern United States (SWUS; Supplementary Fig. S1), drought impacts on forests have been relatively severe since the late 1990s (refs 5,11). This period has been punctuated by the highest temperatures in the observed record, positively influencing atmospheric moisture demand[12]. The ongoing heat-driven drought, in combination with a multitude of ecophysiological data documenting regional forest processes, makes the SWUS an ideal natural experimental target[13] for examining the influence of heat-induced drought on productivity and tree mortality in drought-sensitive forests.

Climate modelling experiments collectively project the SWUS to become warmer and more arid as greenhouse-gas concentrations rise and the sub-tropical high-pressure zones expand and shift polewards[14,15]. Water balance has long been known to substantially limit tree growth and influence forest disturbances in the SWUS; however, the relative importance of temperature and precipitation requires clarification[16]. Temperature should be expected to influence water balance because it exponentially influences atmospheric evaporative demand (Supplementary Fig. S2). Uncertainty regarding the relative roles of evaporative demand versus precipitation in dictating forest drought-stress and tree mortality has limited our

ability to anticipate future impacts to forests, which might otherwise be estimated through global climate model output. Here we develop a tree-ring-based index of forest drought-stress that explicitly resolves the contributions of the vapour-pressure deficit (VPD; difference between the actual- and saturation-vapour pressure, largely controlled by temperature) and precipitation. We link this index to the most comprehensive set of regional forest productivity and disturbance records assembled so far. We use an ensemble of climate-model projections of VPD and precipitation to project future levels of forest drought-stress and place them in the context of historic events known to have caused widespread tree mortality.

Forest drought-stress and climate

Annual tree-ring widths reflect variability in the environmental stressors that limit growth[17]. We used tree-ring records to develop an index of annual forest stress for dominant southwestern tree species, AD 1000–2007. The index is based on 335 collections of site-specific tree-ring width measurements (13,147 specimens) from throughout the SWUS and surrounding regions (Supplementary Fig. S1; see Supplementary Information for all methods and data sources). Nearly all chronologies represent the three most abundant conifer species in the SWUS: piñon (*Pinus edulis*), ponderosa pine (*P. ponderosa*) and Douglas-fir (*Pseudotsuga menziesii*). Sites reflect a range of elevations along landscape moisture gradients.

We call the first-principal-component time series of ring-width chronologies the SWUS FDSI (Fig. 1a) because it is highly representative of interannual variability in ring width across

[1]Earth & Environmental Sciences Division, Los Alamos National Laboratory, Los Alamos, New Mexico 87545, USA, [2]US Geological Survey, Fort Collins Science Center, Jemez Mountains Field Station, Los Alamos, New Mexico 87544, USA, [3]School of Geography and Development, University of Arizona, Tucson, Arizona 85721, USA, [4]Laboratory of Tree-ring Research, University of Arizona, Tucson, Arizona 85721, USA, [5]Theoretical Division, Los Alamos National Laboratory, Los Alamos, New Mexico 87545, USA, [6]Lamont-Doherty Earth Observatory of Columbia University, Palisades, New York 10964, USA, [7]Laboratory of Tree-Ring Science, Department of Geography, The University of Tennessee, Knoxville, Tennessee 37996, USA, [8]Space Data Systems, Los Alamos National Laboratory, Los Alamos, New Mexico 87545, USA. *e-mail: parkwilliams@lanl.gov.
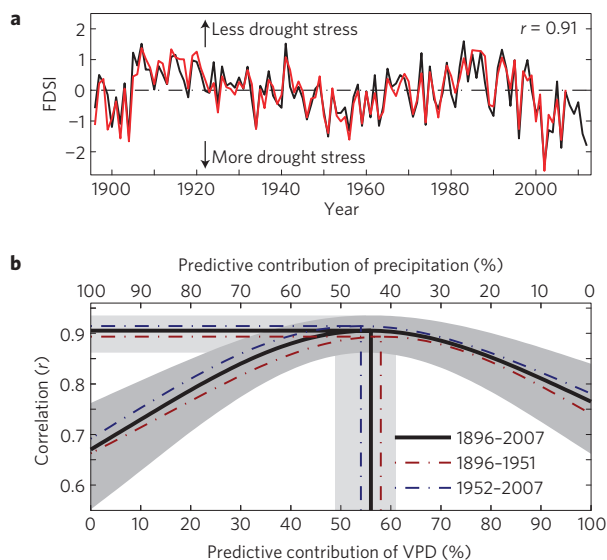
Figure 1 | Correlation between the FDSI and climate. a, The annual FDSI derived from tree ring-width index records (red, 1896–2007) and estimated with climate data using equation (1) (black, 1896–2012). See Supplementary Fig. S3 for estimated confidence ranges in the FDSI values. **b**, Curves show correlation between the estimated and the actual FDSI, allowing predictive contributions of the warm-season VPD and cold-season precipitation to vary from 0 to 100% and 100 to 0%, respectively. The straight lines connect optimal correlations with axes. Grey areas represent 95% confidence intervals.

space and species (Supplementary Fig. S1) and because the index correlates well with observed drought-related climate variables. See Supplementary Fig. S3 for sample size and error. The FDSI is unique because it explicitly represents regionally coherent tree-growth variability calculated from all available ring-width records from the three main conifer species in the SWUS. In contrast, climate-reconstruction approaches (for example, ref. 18) are tuned to represent a specific drought variable during a specific season, using only ring-width records that correlate well with the drought variable of interest.

Considering observed climate data during 1896–2007, the FDSI most strongly correlates with the log of cold-season precipitation (positive relationship) and the warm-season VPD (a combination of the previous August–October and growing-season May–July VPD, negative relationship). The FDSI can be estimated using the following formula:

$$\text{Estimated FDSI} = 0.44[\text{zscore}(\ln(P_{ndjfm}))]$$

$$- 0.56[\text{zscore}((VPD_{aso} + VPD_{mjj})/2)] \quad (1)$$

where the subscripts are the initials of months, underlined initials indicate months of the previous year, and zscore indicates time-series standardization so values during 1896–2007 have a mean of zero and a standard deviation of one (Supplementary Information). Coefficients in equation (1) indicate that the warm-season VPD and cold-season precipitation (P) account for 56% and 44% of the predictive power, respectively (derived visually in Fig. 1b). Combined, these variables account for 82% of the tree-ring-derived FDSI variability ($p < 0.0001$, 95% confidence: $0.74 \le R^2 \le 0.88$). Relative contributions of the warm-season VPD and cold-season precipitation were stable throughout the instrumental period (Fig. 1b).

The seasons when precipitation and the VPD are best correlated with the FDSI are consistent with our knowledge of plant physiology. Stemwood growth in the SWUS is most

strongly dependent on soil–water recharge from cold-season precipitation[13,19,20]. Warming in spring and summer causes the VPD to increase exponentially (Supplementary Fig. S2) and soil moisture decreases through evapotranspiration. Increased VPD coupled with limited soil moisture increases the potential for hydraulic failure (collapse of water columns within xylem cells) and can force prolonged stomatal closure, decreasing photosynthesis, growth rate and carbohydrate reserves[16,21,22]. Correlation between growth and the VPD does not extend into August, consistent with observations of a mid- to late-summer shutdown of radial growth among SWUS trees (for example, refs 17,19). Instead, the FDSI is negatively correlated with the August–October VPD of the previous year. Although these months are not entirely within the warm season, the mechanisms by which the previous autumn VPD limits tree growth are similar to those of the warm season. When conditions allow, photosynthesis continues during August–October after cambial shutdown, allowing allocation of carbohydrates to reserves that influence radial growth during the following growing season[17]. The VPD during this period can also influence soil-moisture recharge by subsequent cold-season precipitation[17].

The FDSI reflects variability in regional-scale vegetation growth, as supported by the strong correlation between the FDSI and the satellite-derived regional normalized difference vegetation index (NDVI) during 1981–2012 (Fig. 2a). The FDSI and NDVI both capture ongoing decline in productivity following the mid-1990s as well as a minimum in 2002. Turn-of-the-century drought conditions reduced productivity and ecosystem uptake of atmospheric carbon throughout western North America[10].

Tree mortality

Ongoing drought-driven decline in regional productivity is associated with widespread tree mortality in the SWUS. Considering the three focal species in this study, FDSI and NDVI minima in 2002 were followed by an approximate doubling of the proportion of dead individuals in the SWUS (Fig. 2b). Other studies[5,23,24] document widespread post-2002 mortality for piñon, which occupies the most arid habitat of the three focal species, but the same is true for ponderosa pine and Douglas-fir.

Much of the conifer mortality in the 2000s was caused by factors influenced by bark-beetle attack and wildfire[9,11,13,25–28]. Bark-beetle populations seem to grow during relatively warm periods and specifically target drought-stressed trees with weakened defences[9,25]. Considering aerial survey data for 1997–2011, we find a negative temporal correspondence between the 2-year running FDSI and the SWUS area that experienced bark-beetle-induced mortality of at least 10 trees per acre (Fig. 2c). Although a longer record is needed to confirm the relationship between the FDSI and beetle-induced tree mortality, the multi-year relationship between the area impacted by bark beetles and the FDSI makes sense because bark-beetle populations grow and decline over multiple seasons[25]. Importantly, the logarithmic scale of the left-hand y axis in Fig. 2c suggests that incremental increases in drought conditions promote exponential increases in the potential for beetle-induced tree mortality. SWUS bark-beetle outbreaks may also be influenced by forest-stand density, which has generally increased in the past century owing to forest management practices[13,29–32].

Our results also indicate a strong exponential correspondence between forest drought-stress and satellite measurements of forest and woodland area burned by wildfire (Fig. 2d). This is consistent with regional analyses of fire scars left on tree rings before observed records (for example, refs 13,26,33). Using SWUS fire-scar data from a network of sites more than four times as dense as those used by previous studies (for example, ref. 13), we find that the probability of an extensive wildfire year in the SWUS was exponentially related to the FDSI during AD 1650–1899 (Fig. 2d inset). These analyses indicate that
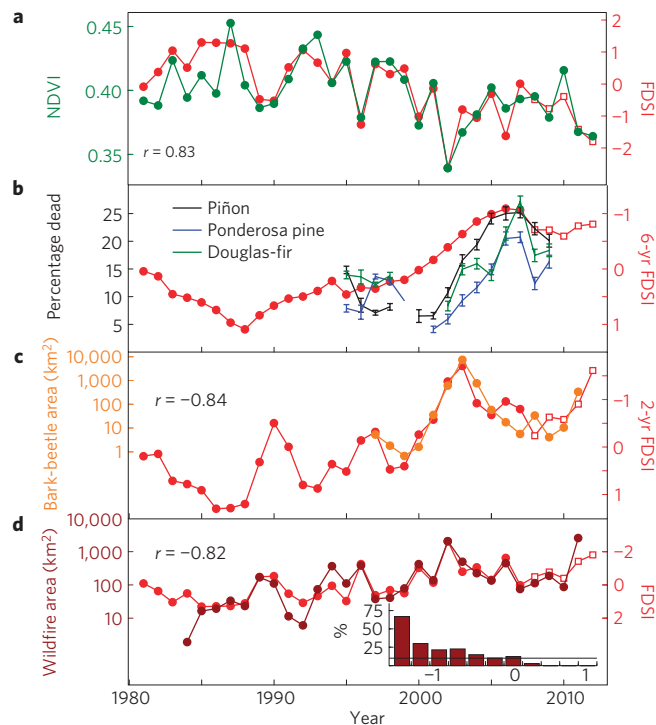
Figure 2 | Measurements of forest productivity and mortality overlaid on the FDSI (red, right *y* axis). a, The annual average late-June to early-August NDVI calculated from satellite (1981–1999: AVHRR, 2000–2012: MODIS) imagery. **b**, Annual forest inventory and analysis measurements of the percentage of standing dead trees in the SWUS for the three most common conifer species. Error bars represent standard deviation of the percentage dead when each year's forest inventory and analysis measurements are randomly resampled 1,000 times (Supplementary Information). **c**, Aerial-survey-derived estimates of the area where ≥ 10 trees per acre were killed by bark-beetle attack. **d**, Satellite-derived moderately and severely burned forest and woodland area in the SWUS. See Supplementary Information and Supplementary Fig. S4 for methods to calculate burned area. The inset shows the percentage of years within a given FDSI class that were top-10% fire-scar years during AD 1650–1899 (the horizontal line is at the expected frequency of 10%, bins are 0.25 FDSI units wide). In all panels, the FDSI values for 2008–2012 (open red squares) were estimated by applying climate data to equation (1). Note the inverted *y* axes for the FDSI in **b–d**.

drought has been, and remains, a primary driver of widespread wildfires in the SWUS.

Given the exponential relationships established between the FDSI and tree mortality, severe drought events before the observed record probably coincided with widespread tree mortality. As observed climate and mortality data are unavailable for much of the past millennium, we use the FDSI record to identify other severe drought events likely to have caused widespread mortality since AD 1000 (Fig. 3). A drought event is defined as any period greater than three years when the mean FDSI is negative, the FDSI is not positive for two consecutive years[34], and the FDSI is less than two standard deviation units below the 1896–2007 mean for at least one year. Drought-event strength is the sum of the FDSI values during the event. Updating the FDSI for 2008–2012 with the FDSI values estimated from equation (1), three drought events have occurred within the observed climate record: the present drought (2000–2012, the fifth strongest since AD 1000), 1945–1964 (the sixth strongest) and 1899–1904 (the seventeenth strongest; Fig. 3). The prolonged 1945–1964 event was indeed associated with extensive tree mortality in the SWUS as indicated by documentation
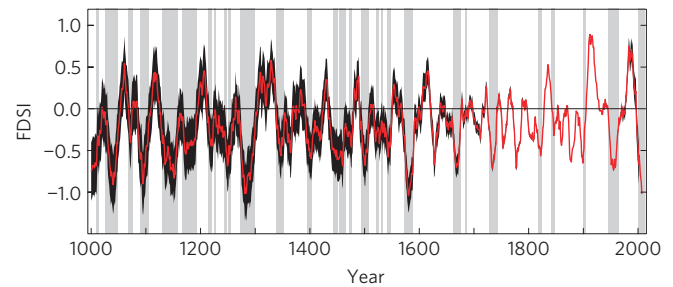

Figure 3 | Eleven-year smoothed FDSI for AD 1000–2012. Black area: 95% confidence range of the FDSI, representing the range of FDSI values expected if all 335 chronologies were available. Vertical grey areas highlight drought events.

of bark-beetle outbreaks[30,35], anomalously large wildfires[31,32] and widespread die-off of conifers[30,31,35]. The 1899–1904 drought was also associated with forest declines[36], although little documented.

Before the 1900s, the 1572–1587 event was the most recent event exceeding the severity of the present event (Fig. 3). This megadrought event[37,38] ranks as the fourth most severe since AD 1000 and the most severe since 1300. Although direct mortality observations are not available for the 1500s event, studies of forest age structure document a scarcity of trees on today's landscape that began growing before the late 1500s (refs 13,31). As lifespans of SWUS conifers often greatly exceed 400 years, the scarcity of trees preceding the 1500s event indicates that intense drought conditions probably led to deaths of a large proportion of trees living at the time. Before the late 1500s, the correspondence between records of conifer pollen buried at archaeological sites and tree-ring widths[39] suggests that widespread tree mortality (indicated by pollen) co-occurred with massive droughts in the 1200s (indicated by tree rings). Notably, ancient Puebloan populations and land-use practices were in great flux during this time, confounding the attribution of a dominant cause of the 1200s forest decline[40].

Future forest drought-stress

The ongoing VPD-dominated drought event (Fig. 4a) is consistent with climate-model projections (phase 3 of the Coupled Model Intercomparison Project (CMIP3)) of increasing warm-season VPD (~3.6% decade^{-1}) throughout the rest of the twenty-first century in response to business-as-usual greenhouse-gas emissions scenarios[41] (SRES A2; Fig. 4a and Supplementary Fig. S6 for alternative emissions scenarios: SRES A1B and B1). Dynamically downscaled (0.5° geographic resolution) model projections indicate similar increases in the VPD (Fig. 4a and Supplementary Information). Furthermore, most models project a slight decrease in cold-season precipitation during the second half of this century (~ − 1.25% decade^{-1}, Fig. 4c). Applying model projections to equation (1), all models indicate negative FDSI trends throughout the twenty-first century (Fig. 4d). By 2050, the ensemble mean FDSI is consistently more severe than that of any megadrought since at least AD 1000 (megadrought conditions are surpassed by 2070 in the most optimistic B1 emissions scenario, Supplementary Fig. S6d). Notably, projections of the FDSI are more severe than projections of gross water balance (precipitation–evaporation) because water-balance projections are influenced more by decreased cold-season precipitation than by increased warm-season VPD (ref. 15).

FDSI projections suggest that SWUS forest drought-stress is entering a new era where natural oscillations such as those apparent in Fig. 3 are superimposed on, and overwhelmed by, a trend towards more intense drought stress. As the VPD diverges from the range of observed variability, nonlinear effects may alter drought impacts on forests (for example, Fig. 5 in ref. 42). During the observed record, equation (1) was a better predictor of the FDSI
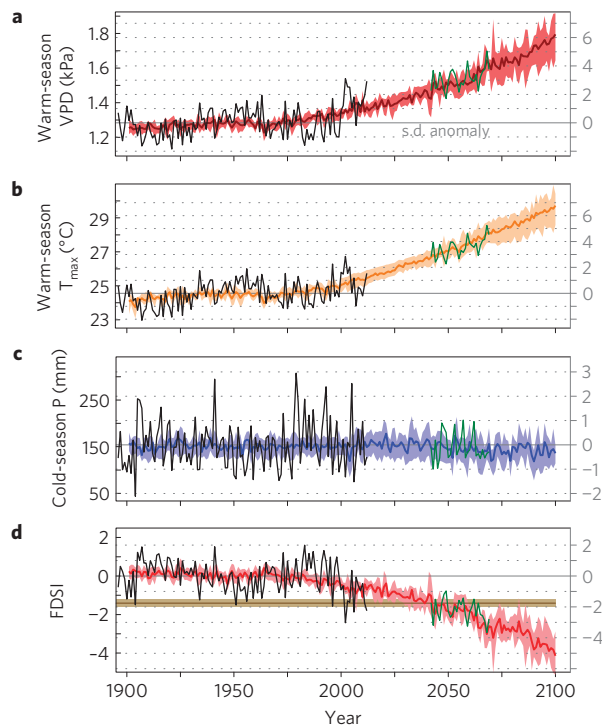
Figure 4 | Observed and modelled climate and forest drought-stress. a–d, The warm-season VPD (**a**), warm-season T_{max} (**b**), cold-season precipitation (**c**) and the FDSI (**d**). Black: observed records. Coloured bold lines: CMIP3 ensemble mean values. Shading around time series: inner 50% of CMIP3 values. Green time series: 2042–2069 dynamically downscaled NARCCAP ensemble mean values. Horizontal brown line and shading in **d** show the mean and 95% confidence FDSI values of the most severe 50% of years during the 1572–1587 megadrought. The horizontal grey lines show the anomaly in standard deviations from the observed 1896–2007 mean (right y axis). See Supplementary Figs S5 and S6 for individual model projections and alternative emissions scenarios.

in years of relatively high drought-stress (Supplementary Fig. S7). This may indicate that forest sensitivity intensifies as drought intensifies, consistent with exponential relationships between the FDSI and tree mortality (Fig. 2c,d). Interestingly, the observed intensification of drought sensitivity during high drought-stress years was mainly due to heightened sensitivity to variability in cold-season precipitation (Supplementary Fig. S7a,b,g). This may mean that cold-season precipitation will gain relative importance as drought intensifies in the coming decades. To account for this and other possible nonlinear effects, we estimated the future FDSI where the relative predictive contributions of cold-season precipitation and the warm-season VPD are forced to vary. Reducing the future predictive contribution of the warm-season VPD to 25%—less than half the observed contribution—and increasing the contribution of cold-season precipitation to 75%, the ensemble mean FDSI is still estimated to equal or exceed 1500s megadrought levels by the 2060s in a business-as-usual emissions scenario (Supplementary Fig. S8a). In the hypothetical case that climate models have over-predicted VPD trends by a factor of two, possibly influenced by model misrepresentation of SWUS monsoon characteristics, megadrought levels are still surpassed during the late twenty-first century (Supplementary Fig. S8d).

Importantly, forest-decline events are particularly sensitive to extreme conditions (Fig. 2c,d). As widespread forest decline seems to have occurred during the 1572–1587 megadrought, we treat the mean FDSI during the most extreme half of the years during this period as a forest-stress benchmark signifying a level of extreme
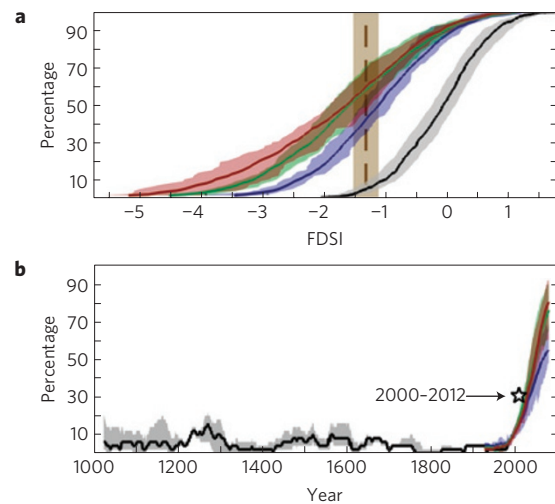

Figure 5 | Extreme drought stress. a, Cumulative distribution functions of tree-ring derived FDSI during AD 1000–2007 (black) and model-projected FDSI during AD 2000–2100 for the A2 (red), A1B (green) and B1 (blue) emissions scenarios. Brown line: mean FDSI during the most extreme half of the 1572–1587 megadrought. **b**, Fifty-year running frequency of annual FDSI values more negative than the mean FDSI during the most negative half of the years during the 1572–1587 megadrought. The colours in **b** represent the same as in **a**. Shaded areas: 95% confidence ranges for tree-ring-derived values and inner-quartile values for model ensemble projections.

drought-stress likely to correspond with widespread forest decline (benchmark FDSI = −1.41). Although the 1200s megadrought was longer, the 1500s megadrought was more extreme. During AD 1000–2007, 4.8% of the FDSI values were more negative than the 1500s benchmark, and the highest 50-year frequency of benchmark years was 18% during 1247–1296. During the present drought event, 4 of the 13 years (31%) qualify as benchmark years. On the basis of ensemble mean projections, 59% of years will be benchmark years during 2000–2100 assuming the A2 emissions scenario (Fig. 5a), and the frequency of benchmark years is projected to reach approximately 80% during the second half of this century (Fig. 5b). Assuming the most optimistic emissions scenario (B1), this value is 53%. Very extreme FDSI values of less then −3 (unprecedented during 1000–2012) are projected to occur with a frequency of approximately 20% in the twenty-first century (A2 scenario, Fig. 5b).

Projections of increased forest drought-stress and tree mortality are relevant throughout the SWUS, not only to the most drought-prone sites. Recent bark-beetle- and wildfire-induced tree mortality has occurred approximately uniformly among a wide variety of SWUS sites ranging from very drought prone to less drought prone than average (Fig. 6a,b; see Supplementary Methods). Mortality has been less common within the ∼20% of forest area least prone to drought (high cold-season precipitation, low warm-season VPD). Observed exponential relationships between the FDSI and forest-decline processes suggest that less drought-prone SWUS forests may become progressively more vulnerable to forest decline processes and mortality as the warm-season VPD increases. Furthermore, regeneration of common conifer species in the SWUS generally occurs in pulses linked to wet/cool conditions[13], and often requires the presence of parent tree sources[32]. Loss of mature trees across increasingly large areas due to high-severity fires and bark-beetle-induced mortality (Fig. 2c,d and Supplementary Fig. S9b), coupled with ongoing and projected increases in drought stress due to climate change (Fig. 4), means that species-specific tree regeneration needs are increasingly less likely to be met after disturbance[43]. This increases the risks of long-term forest structural
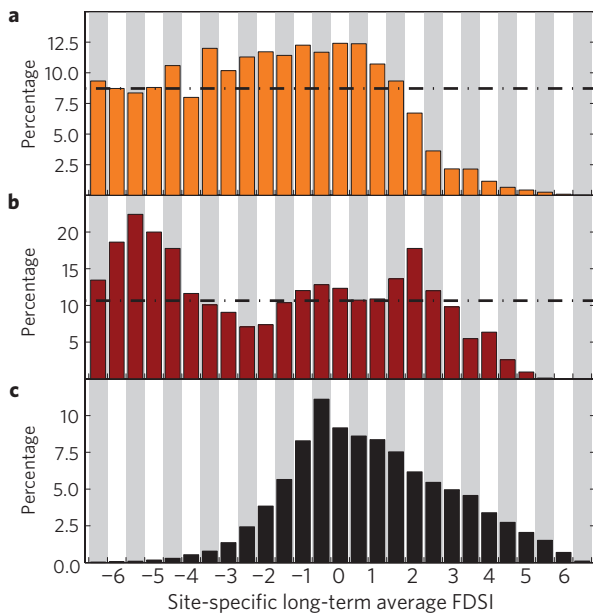
Figure 6 | Where have trees died? The *x* axis represents a long-term drought-stress gradient among SWUS forest grid cells. The grid cells with the most severe long-term drought-stress are on the left side of plots. **a**, The percentage of grid cells in each drought-stress class with ≥ 10 trees per acre killed by bark beetles during 1997–2011. **b**, The percentage of grid cells in each drought-stress class where moderate or severe wildfire occurred during 1984–2011. Horizontal dotted black lines in **a** and **b** indicate expected percentages if these mortality processes were spatially uniform. **c**, Probability distribution function of the average FDSI during 1896–2007 among SWUS forest grid cells. The site-specific FDSI (*x* axis) estimated using equation (1). The methods are described in the Supplementary Information. Grey and white shading is intended to assist with interpretation.

and compositional changes and type conversions from forests to shrublands or grasslands (for example, refs 32,44).

Conclusions

The warm-season VPD was at least as important as cold-season precipitation in dictating SWUS forest drought-stress during 1896–2007. The warm-season VPD has been particularly high since 2000 and is the primary driver of an ongoing drought-stress event that is more severe than any event since the late 1500s megadrought. The present event has been associated with regional-scale declines in canopy greenness and tree survival, due in part to large bark-beetle outbreaks and increasingly large wildfires. On the basis of an ensemble of climate-model projections, continued increases in the warm-season VPD will by the mid-twenty-first century force mean annual SWUS forest drought-stress levels to exceed the severity of the strongest megadroughts since at least AD 1000. Importantly, the warm-season VPD is largely driven by the maximum daily temperature (T_{max}) in the SWUS. As such, warm-season T_{max} is nearly as effective as the warm-season VPD at predicting the FDSI (Supplementary Fig. S10). The importance of the VPD and temperature in dictating the FDSI, combined with the relatively high confidence in the projections of continued warming in the SWUS (ref. 45), translates into a high confidence in projections of intensified forest drought-stress. The strong correspondence between forest drought-stress and tree mortality suggests that intensified drought-stress will be accompanied by increased forest decline. Importantly, human forest-management practices have profoundly influenced the regional wildfire regime over the past century[46] and future practices will continue to influence the impacts

of drought on wildfire behaviour. Furthermore, there are many complex interactions not accounted for in this study, including interactions between disturbance processes[29]. We therefore constrain our quantitative projections to the FDSI and do not forecast absolute magnitudes of forest area impacted by bark beetles or wildfire.

The implications of this study extend beyond the well-studied SWUS region. Given that the ongoing SWUS drought event is probably a product of both natural and anthropogenic forcing[47], it serves as a natural experiment where the recent forest response to drought may serve as a harbinger of how drought-sensitive forests globally may respond to warming[1], with implications regarding terrestrial carbon budgets[10]. Model projections[48,49] and observations[50] of a poleward expansion of the subtropics indicate that forests near the poleward edges of the subtropics may be particularly vulnerable to enhanced drought-induced tree mortality. This study indicates that if warming continues, increasing VPD and drought stress will continue to cause twenty-first-century readjustments to the SWUS forest structure, composition and distribution through amplified disturbance processes that have become increasingly evident regionally in recent decades (for example, Supplementary Fig. S9). Given the reproductive and dispersal limitations of dominant native tree species, climate-driven amplification of forest drought-stress and associated disturbance processes can be expected to force many landscapes in the SWUS and probably elsewhere towards vegetation-type conversions, with species distributions quite different from those familiar to modern civilization.

References

1. Allen, C. D. *et al.* A global overview of drought and heat-induced tree mortality reveals emerging climate change risks for forests. *Forest Ecol. Manage.* **259**, 660–684 (2010).
2. Zhao, M. & Running, S. W. Drought-induced reduction in global terrestrial net primary production from 2000 through 2009. *Science* **329**, 940–943 (2010).
3. Van Mantgem, P. J. *et al.* Widespread increase of tree mortality rates in the western United States. *Science* **323**, 521–524 (2009).
4. Beck, P. S. A. *et al.* Changes in forest productivity across Alaska consistent with biome shift. *Ecol. Lett.* **14**, 373–379 (2011).
5. Breshears, D. D. *et al.* Regional vegetation die-off in response to global-change-type drought. *Proc. Natl Acad. Sci. USA* **102**, 15144–15148 (2005).
6. Phillips, O. L. *et al.* Drought sensitivity of the Amazon rainforest. *Science* **323**, 1344–1347 (2009).
7. Lewis, S. L., Brando, P. M., Phillips, O. L., van der Heijden, G. M. F. & Nepstad, D. The 2010 amazon drought. *Science* **331**, 554 (2011).
8. Peng, C. *et al.* A drought-induced pervasive increase in tree mortality across Canada's boreal forests. *Nature Clim. Change* **1**, 467–471 (2011).
9. Bentz, B. J. *et al.* Climate change and bark beetles of the western United States and Canada: Direct and indirect effects. *Bioscience* **60**, 602–613 (2010).
10. Schwalm, C. R. *et al.* Reduction in carbon uptake during turn of the century drought in western North America. *Nature Geosci.* **5**, 551–556 (2012).
11. Williams, A. P. *et al.* Forest responses to increasing aridity and warmth in the southwestern United States. *Proc. Natl Acad. Sci. USA* **107**, 21298–21294 (2010).
12. Weiss, J. L., Castro, C. L. & Overpeck, J. T. Distinguishing pronounced droughts in the southwestern United States: Seasonality and effects of warmer temperatures. *J. Clim.* **22**, 5918–5931 (2009).
13. Swetnam, T. W. & Betancourt, J. L. Mesoscale disturbance and ecological response to decadal climatic variability in the American Southwest. *J. Clim.* **11**, 3128–3147 (1998).
14. Diffenbaugh, N. S., Ashfaq, M. & Scherer, M. Transient regional climate change: Analysis of the summer climate response in a high-resolution, century-scale ensemble experiment over the continental United States. *J. Geophys. Res.* **116**, D24111 (2011).
15. Seager, R. *et al.* Model projections of an imminent transition to a more arid climate in southwestern North America. *Science* **316**, 1181–1184 (2007).
16. McDowell, N. G. *et al.* Mechanisms of plant survival and mortality during drought: Why do some plants survive while others succumb to drought? *New Phytol.* **178**, 719–739 (2008).
17. Fritts, H. C. *Tree Rings and Climate* (Academic, 1976).
18. Cook, E. R., Woodhouse, C. A., Eakin, C. M., Meko, D. M. & Stahle, D. W. Long-term aridity changes in the western United States. *Science* **306**, 1015–1018 (2004).

19. McDowell, N. G., Allen, C. D. & Marshall, L. Growth, carbon-isotope discrimination, and drought-associated mortality across a *Pinus ponderosa* elevational transect. *Glob. Change Biol.* **16,** 399–415 (2010).
20. St. George, S., Meko, D. M. & Cook, E. R. The seasonality of precipitation signals embedded within the North American Drought Atlas. *Holocene* **20,** 983–988 (2010).
21. Adams, H. D. *et al.* Temperature sensitivity of drought-induced tree mortality portends increased regional die-off under global change-type drought. *Proc. Natl Acad. Sci. USA* **106,** 7063–7066 (2009).
22. McDowell, N. G. *et al.* The interdependence of mechanisms underlying climate-driven vegetation mortality. *Trends Ecol. Evol.* **26,** 523–532 (2011).
23. Shaw, J. D., Steed, B. E. & DeBlander, L. T. Forest inventory and analysis (FIA) annual inventory answers the question: What is happening to pinyon-juniper woodlands? *J. Forestry* **103,** 280–285 (2005).
24. Huang, C., Asner, G. P., Barger, N. N., Neff, J. C. & Floyd, M. L. Regional aboveground live carbon losses due to drought-induced tree dieback in piñon–juniper ecosystems. *Remote Sens. Environ.* **114,** 1471–1479 (2010).
25. Raffa, K. F. *et al.* Cross-scale drivers of natural disturbances prone to anthropogenic amplification: The dynamics of bark beetle eruptions. *Bioscience* **58,** 501–517 (2008).
26. Grissino Mayer, H. D. & Swetnam, T. W. Century scale climate forcing of fire regimes in the American Southwest. *Holocene* **10,** 213–220 (2000).
27. Westerling, A. L., Hidalgo, H. G., Cayan, D. R. & Swetnam, T. W. Warming and earlier spring increase western US forest wildfire activity. *Science* **313,** 940–943 (2006).
28. Furniss, R. L. & Carolin, V. M. *Western Forest Insects* (United States Department of Agriculture (USDA) Forest Service (FS), 1977).
29. Allen, C. D. Interactions across spatial scales among forest dieback, fire, and erosion in northern New Mexico landscapes. *Ecosystems* **10,** 797–808 (2007).
30. Allen, C. D. & Breshears, D. D. Drought-induced shift of a forest-woodland ecotone: Rapid landscape response to climate variation. *Proc. Natl Acad. Sci. USA* **95,** 14839–14842 (1998).
31. Betancourt, J. L., Pierson, E. A., Rylander, K. A., Fairchild-Parks, J. A. & Dean, J. S. in *Managing Piñon-juniper Ecosystems for Sustainability and Social Needs* (eds Aldon, A. F. & Shaw, D. W.) 42–62 (USDA Forest Service, 1993).
32. Savage, M. & Mast, J. N. How resilient are southwestern ponderosa pine forests after crown fires? *Can. J. Forest Res.* **35,** 967–977 (2005).
33. Swetnam, T. W. & Betancourt, J. L. Fire-southern oscillation relations in the southwestern United States. *Science* **249,** 1017–1020 (1990).
34. Herweijer, C., Seager, R., Cook, E. R. & Emilie-Geay, J. North American droughts of the last millennium from a gridded network of tree-ring data. *J. Clim.* **20,** 1353–1376 (2007).
35. Potter, L. D. Phytosociological study of San Augustin Plains, New Mexico. *Ecol. Monogr.* **27,** 114–136 (1957).
36. Plummer, F. G., Rixon, T. F. & Dodwell, A. *Forest Conditions in the Black Mesa Forest Reserve, Arizona. Series H* (Government Printing Office, 1904).
37. Stahle, D. W. *et al.* Tree-ring data document 16th century megadrought over North America. *EOS Trans.* **81,** 121–121 (2000).
38. Grissino-Mayer, H. D. in *Tree Rings, Environment, and Humanity* (eds Dean, J. S., Meko, D. M. & Swetnam, T. W.) 191–204 (Radiocarbon, 1996).
39. Dean, J. S. The medieval warm period on the southern Colorado Plateau. *Climatic Change* **26,** 225–241 (1994).
40. Fall, P. L., Kelso, G. & Markgraf, V. Paleoenvironmental reconstruction at Canyon del Muerto, Arizona, based on principal-component analysis. *J. Archaeol. Sci.* **8,** 297–307 (1981).
41. IPCC *Special Report on Emissions Scenarios* (eds Nakicenovic, N. & Swart, R.) (Cambridge Univ. Press, 2000).
42. Williams, A. P., Michaelsen, J., Leavitt, S. W. & Still, C. J. Using tree rings to predict the response of tree growth to climate change in the continental United States during the twenty-first century. *Earth Interact.* **14,** 1–20 (2010).
43. Jackson, S. T., Betancourt, J. L., Booth, R. K. & Gray, S. T. Ecology and the ratchet of events: climate variability, niche dimensions, and species distributions. *Proc. Natl Acad. Sci. USA* **106,** 19685–19692 (2009).
44. Goforth, B. R. & Minnich, R. A. Densification, stand-replacement wildfire, and extirpation of mixed conifer forest in Cuyamaca Rancho State Park, southern California. *Forest Ecol. Manage.* **256,** 36–45 (2008).
45. Räisänen, J. CO_2-induced climate change in CMIP2 experiments: Quantification of agreement and role of internal variability. *J. Clim.* **14,** 2088–2104 (2001).
46. Marlon, J. R. *et al.* Long-term perspective on wildfires in the western USA. *Proc. Natl Acad. Sci. USA* **109,** E535–E543 (2012).
47. Cayan, D. R. *et al.* Evolution toward greater droughts in the SW United States. *Proc. Natl Acad. Sci. USA* **107,** 21271–21276 (2010).
48. Held, I. M. & Soden, B. J. Robust responses of the hydrological cycle to global warming. *J. Clim.* **19,** 5686–5699 (2006).
49. Seager, R., Naik, N. & Vecchi, G. A. Thermodynamic and dynamic mechanisms for large-scale changes in the hydrological cycle in response to global warming. *J. Clim.* **23,** 4651–4668 (2010).
50. Seidel, D. J., Fu, Q., RanDel, W. J. & Reichler, T. S. J. Widening of the tropical belt in a changing climate. *Nature Geosci.* **1,** 21–24 (2008).

Acknowledgements

Author contributions

A.P.W., C.D.A., A.K.M., D.G., C.A.W., D.M.M., T.W.S., S.A.R., R.S., M.C. and N.G.M. conceived and designed the experiments. A.P.W. performed the experiments. A.P.W. and E.R.C. analysed the data. A.K.M., D.G., C.A.W., C.G., D.M.M., T.W.S., S.A.R., H.D.G-M., J.S.D. and E.R.C. contributed data. A.P.W., C.D.A., A.K.M., D.G., C.A.W., D.M.M., T.W.S., S.A.R., R.S., H.D.G-M. and N.G.M. wrote the paper.

Additional information

Supplementary information is available in the online version of the paper. Reprints and permissions information is available online at www.nature.com/reprints. Correspondence and requests for materials should be addressed to A.P.W.

Competing financial interests

The authors declare no competing financial interests.